2016

Prediction of Air-Side Particulate Fouling of HVAC&R Heat Exchangers

H. Inamdar
Purdue University

E. A. Groll
Purdue University

J. A. Weibel
Purdue University, jaweibel@purdue.edu

S V. Garimella
Purdue University, sureshg@purdue.edu

Inamdar, H.; Groll, E. A.; Weibel, J. A.; and Garimella, S V., "Prediction of Air-Side Particulate Fouling of HVAC&R Heat Exchangers" (2016). *CTRC Research Publications.* Paper 307.
http://dx.doi.org/http://dx.doi.org/10.1016/j.applthermaleng.2016.05.082

Prediction of Air-Side Particulate Fouling of HVAC&R Heat Exchangers

Harshad V. Inamdar[(a)], Eckhard A. Groll[(a)], Justin A. Weibel[(b)], Suresh V. Garimella[(b)]

[(a)] Purdue University, School of Mechanical Engineering,
Ray W. Herrick Laboratories and Cooling Technologies Research Center, West Lafayette, IN 47907 USA

[(b)] Purdue University, School of Mechanical Engineering,
Cooling Technologies Research Center, West Lafayette, IN 47907 USA

ABSTRACT

Air-to-refrigerant heat exchangers used in heating, ventilation, air-conditioning, and refrigeration systems routinely experience air-side fouling due to the presence of particulates in outdoor and indoor environments. The influence on the performance of the heat exchanger, in terms of heat transfer efficiency and pressure drop imposed, depends on the extent of air-side fouling. Fouling of a heat exchanger is determined by a variety of parameters such as the dimensions of the heat exchanger, physical properties of the airborne particulates, and airflow conditions over the heat exchange surfaces. A comprehensive model is developed to deterministically calculate the extent of fouling of a heat exchanger as a function of these parameters by accounting for each of the possible deposition mechanisms. The study enhances modeling approaches previously employed in the literature by accounting for time-dependent accumulation of particles as well as the effects of the streamwise distribution of accumulated dust on subsequent fouling; the calculations for the deposition due to several of the mechanisms are also refined to improve prediction accuracy. Particulate matter deposits already present on the surface are found to accelerate the process of fouling by decreasing available area for airflow; an existing deposit layer effectively decreases the distance that a particle must travel to collide with a surface and increases the surface area available for deposition. The modified model predictions are compared against extant experimental deposition fraction data; an improved agreement is observed compared to previous models in the literature.

Keywords: particulate matter, heat exchanger, air-side fouling, HVAC&R

1. INTRODUCTION

Fouling of heat exchangers can have serious detrimental effects and has been investigated extensively. A majority of this effort has focused on understanding the phenomenon of tube-side fouling (fouling on the inside surfaces of tubes) [1]. Air-side fouling of heat exchangers (fouling on the outside surfaces of tubes) occurs as a result of sedimentation and deposition of particulate matter suspended in air. This particulate matter is usually composed of coarse and fine dust, fibers, and other pollutants present in the air [2]. Compared to tube-side fouling, prediction and assessment of air-side fouling is complicated by the variety of particulate types potentially present in the air stream, the irregular outer fin and tube surface geometries, and the dependence of the deposition mechanisms on these factors. Prediction of air-side fouling must thus account for the influences of a large number of parameters including the heat exchanger geometry, thermodynamic and transport characteristics of the airflow, and properties of the particulates suspended in the air stream.

2. LITERATURE REVIEW

One of the earliest attempts to experimentally characterize air-side fouling of heat exchangers with complex fin and tube surface geometries was reported by Bott and Bemrose [3], who experimentally fouled a four-row, four-pass, spiral-wound finned tube heat exchanger using precipitated calcium carbonate dust. The tests performed indicated that the Colburn-*j* factor and friction factor of the heat exchanger were influenced by fouling. The ratio of the instantaneous friction factor to its initial value asymptotically reached a constant value with progressive fouling. The

difficulty in predictive modeling of such air-side fouling behavior, specifically at the scale of a complete heat exchanger, has hindered the development of universal models. Instead, heat exchanger fouling models are developed based on related studies that investigate fouling of representative heat transfer surfaces, and focus on one or two selected deposition mechanisms. Thus, reasonable accuracy can only be expected when modeling fouling of these specific surfaces under certain operating conditions for which the predominant deposition mechanisms are captured.

Waldmann and Schmitt [4] modeled the thermophoresis and diffusiophoresis of aerosols and provided analytical expressions for the corresponding particle velocities. Goldsmith and May [5] experimentally measured particle deposition due to these mechanisms on flat plates. A test section was constructed out of two parallel plates between which a temperature or water-vapor gradient was maintained as necessary. Derjaguin *et al.* [6] also modeled diffusiophoresis and thermophoresis of aerosol particles. These analyses were valid both for small particles (particle radius smaller than the mean free path of gas molecules) which were assumed to not affect the flow field in their vicinity, and for large particles (particle radius much larger than the mean free path) which do affect the gas flow field around them. Annis *et al.* [7] extended the range of applicability of earlier diffusiophoresis models specifically for particle radii on the same order of magnitude as the mean free path of the gas molecules. Pilat and Prem [8] used the models developed by Waldmann and Schmitt [4] to analyze particle collection efficiency of a water droplet due to thermophoresis and diffusiophoresis, in addition to the effects of inertial impaction and Brownian diffusion.

Davies [9] first analyzed particle deposition due to turbulence by modeling particle transport from the bulk fluid to the boundary layer by turbulent diffusion followed by deposition in the laminar sublayer under free flight. Sehmel [10, 11, 12] modeled turbulent deposition of particles from boundary layers adjacent to the surface. An important contribution was the inclusion of particle eddy diffusivities; it was found from experimental data that particle eddy diffusivity was greater than the fluid eddy diffusivity due to turbulence. Cleaver and Yates [13] analyzed the deposition of particles by modeling their transport across the viscous sub-layer in a turbulent boundary layer. They also accounted for re-entrainment of particles by analyzing the local wall shear stress and turbulent bursts, and analyzed the limiting cases of gravity-dominated and inertia-dominated deposition. Later advances leveraged numerical modeling approaches, such as the study by Kallio and Reeks [14] who calculated particle trajectories in turbulent boundary layers to calculate particle deposition velocities in pipe flow.

Based on the foundational models discussed above that considered deposition due to individual mechanisms, comprehensive fouling models were developed for more realistic situations and flow geometries. Epstein [15] modeled the phenomenon of particulate fouling of flat heat transfer surfaces due to various individual particle deposition mechanisms. The paper reviewed the different mechanisms of particle deposition driven by diffusion, inertia, impaction, gravitational settling, and thermophoresis, and presented analytical models to calculate the deposition velocity of particles for each mechanism. Bott [16] used a deposition velocity to model fouling of heat exchangers, with this velocity being defined as the mass flux of particles from the bulk flow to the surface on which deposition is being analyzed for fouling, normalized by the aerosol concentration. The transport of particles was separated into two types of phenomena: transport across the bulk flow region toward the boundary layer and surface (Brownian motion, eddy diffusion, and thermophoresis), and transport across the boundary layer to adhere to the surface (particle diffusion, inertial impaction, and thermophoresis). The lack of good-quality experimental data was identified as a limitation for assessment of the model accuracy and simplifying assumptions made.

Siegel and Nazaroff [17] accounted for the individual mechanisms described above and developed a model to predict deposition of particles in a diameter range of 0.01 to 100 μm on wavy fin-tube heat exchangers. The contribution of each deposition mechanism to the overall deposition fraction was deterministically calculated, except in the case of deposition due to turbulence, where a Monte Carlo simulation method was utilized. Experiments were conducted to measure the deposition fractions of monodisperse oil particles at different air velocities. The model predicted Brownian motion to be the dominant deposition mechanism for particles in the diameter range of 0.01-1 μm, while impaction on the leading edge of fins was predicted to be dominant in the 1-10 μm range. For the range of 10-100 μm, gravitational settling, impaction on tubes, and deposition due to turbulence were all contributing factors. The model showed qualitative agreement with experimental data, but underpredicted the extent of fouling at higher velocities and for larger particles.

The current work extends previous modeling approaches to include additional deposition characteristics in order to better represent the physical situation and improve prediction accuracy. In particular, the modeling enhancements include superimposition of the different fouling mechanisms, prediction of the distribution of deposits on the heat

exchanger surface along the streamwise direction, analysis of the effects of accumulated deposits on subsequent fouling, and adaption of the previous modeling approach to different heat exchanger geometries. A comparison of model predictions with published experimental data is presented.

3. MODEL DESCRIPTION

The current modeling approach builds upon the deposition mechanisms considered by Siegel and Nazaroff [17]. The Siegel and Nazaroff [17] (SN) model accounted for fouling of heat exchangers through inertial impaction on fins and tubes, gravitational settling, and deposition due to Brownian motion, turbophoresis, thermophoresis, and diffusiophoresis as described below:

i. Inertial impaction on fins and tubes represents the deposition that occurs when particulate matter in air flows around obstacles such as fins and tubes. If the inertia of a particle is high, it may not perfectly follow streamlines of air. The path that the particle moves along may lead to a collision with the obstacle, leading to deposition.
ii. Gravitational settling accounts for deposition of particles under gravity. The larger the mass of a particle, the greater is the displacement due to gravity. If this displacement is large enough, the particle will settle onto the floor of the airflow passage.
iii. Deposition due to Brownian motion accounts for the collision with, and subsequent deposition of, particles on heat exchanger surfaces due to random motion. This random motion, caused by momentum transferred to these particles by collisions with air molecules, is dominant at small particle sizes.
iv. The presence of turbulence in the airflow causes movement of particles away from high-turbulence zones. This is due to a gradient in the momentum transferred to the particles from collisions with air molecules. As the particles move in directions orthogonal to the airflow, they may encounter heat exchanger surfaces and deposit.
v. Thermophoretic deposition also occurs due to a gradient in the momentum transferred to particles due to collisions with air molecules. However, this gradient in the transferred momentum is explained by a temperature gradient present in the airflow as a result of operation of the heat exchanger itself.
vi. Diffusiophoretic deposition occurs due to the motion of particles under the action of diffusive forces. These diffusive forces result from moisture concentration gradients present in the air. As air is heated or cooled, its moisture-bearing capacity changes, causing a change in the moisture concentration. Diffusive fluxes of moisture and air lead to lateral particle motion toward surfaces.

In the SN model, fouling of the tubes and fins of a heat exchanger was modeled for a finite number of distinct particle sizes, and the aggregate particulate deposition was calculated based on the particulate matter composition in the air stream. Using the detailed description of the model published by Siegel [24], the SN model was first replicated to ensure consistency with past efforts. The model was then modified as described in Section 3.3.

3.1 Modeling Assumptions

The following assumptions are applicable to all the fouling mechanisms considered in this model:

i. Dust particles suspended in the air are perfectly spherical solid particles with a known size distribution based on mass;
ii. The effective particle density of the particulate suspension in the air stream can be represented by a weighted mean of the constituent particle densities based on the mixture composition;
iii. The bulk density of the aggregate deposited particulate matter differs from the particle density; neither is a function of operating conditions such as air velocity, air humidity, air temperature, or suspended particulate matter concentration;
iv. Every collision between particles and heat exchanger surfaces is assumed to be perfectly inelastic, *i.e.*, every collision results in adhesion of the particle to the surface, and a separate model for particle adhesion is not implemented;
v. There is no re-entrainment of particles into the air stream after initial deposition;
vi. Deposition occurs on the lateral surfaces of the fins, as well as on the front edges, while the trailing one-quarter area of the tube surfaces remains free of fouling;
vii. No fouling mechanism causes the transport of particles transverse to the bulk streamwise direction in a direction opposite to gravity; and

viii. The particulate suspension in the air stream maintains a uniform spatial distribution as it flows through the heat exchanger, *i.e.*, no spatial gradients exist in the suspended particle concentration.

3.2 Deposition Fraction

Deposition fraction is used to quantitatively evaluate the extent of fouling of the heat exchanger surface. It is a mass-based, non-dimensional number defined as:

$$deposition\ fraction = \frac{mass\ of\ \ dust\ deposited\ on\ the\ heat\ exchanger}{total\ mass\ of\ \ dust\ entering\ the\ front\ face\ of\ \ the\ heat\ exchanger} \tag{1}$$

Conversely, the penetration fraction is a quantity used to evaluate the fraction of particles which are able to pass through the heat exchanger without depositing:

$$penetration\ fraction = 1 - deposition\ fraction \tag{2}$$

3.3 Motivation and Description of Modifications to the Siegel-Nazaroff (SN) Model

A flow chart of the analytical model developed to predict fouling of HVAC&R heat exchangers is presented in Figure 1. The model, implemented in MATLAB, consists of simplified mathematical, deterministic calculations of the deposition fractions for particles of a specific size due to each deposition mechanism (except deposition due to turbulence, which needs a probabilistic calculation). The penetration fractions for each particle size are then calculated and multiplied to find the aggregate penetration fraction for a given particle size. This is possible because all deposition mechanisms (except thermophoresis and diffusiophoresis) are assumed to be independent of one other, which can be justified by the observation that each of the specific mechanisms dominates in unique and discrete ranges of particle size. Figure 2 describes the naming convention used to denote directions relative to the duct. Table 1 lists some of the key equations used in the model to analyze the deposition mechanisms.

3.3.1 Drag force on a particle: We use a correlation for the drag force acting on a particle, given by Haider and Levenspiel [25], that is valid for particle Reynolds numbers up to 2.6×10^5 and also for non-spherical particles. The current model may thus be expanded to account for the deposition of fibers. The SN model used a correlation given by Seinfeld and Pandis [26]. The analysis of flow in the Stokes and Newtonian regimes assumes that the relative velocity of the fluid medium at the surface of the particle is zero, *i.e.*, a no-slip boundary condition. However, for particles whose size approaches the mean free path in the fluid medium, there is slip between the particle and fluid molecules at this surface which reduces the drag force acting on the particle. The Cunningham correction factor is used to account for this slip [27]. The value of the slip correction factor reduces to 1 as the particle size increases. The mean free path in air has been calculated as given by Jennings [27]. The new correlation used to calculate drag force is reflected in equations (7.2) and (8.2) in Table 1.

3.3.2 Zone-based modeling of gravitational settling: Deposition due to gravitational settling is typically accounted for in most prior models, but usually for channels of constant streamwise cross-section. For wavy finned tube heat exchangers, on the other hand, the air is split into paths that flow either through the fin corrugations or through the open spaces between fins. These regions offer different distances for the particle to travel before settling. The settling surface orientations also differ, and hence the two regions must be analyzed separately, as shown in Figure 3. Particulate matter in the open zone (filled in with a cross-hatched pattern) will deposit on the floor of the heat exchanger by gravitational settling after traveling a distance much larger than the pitch of the wavy fins. On the other hand, particulate matter in the fin corrugation zone (shaded solid gray) will deposit on the wavy fins. The maximum distance a particle would travel as it settles under gravity before encountering a surface is on the order of the pitch of the wavy fins. The total deposition by gravitational settling is the sum of the deposition in the two zones. Equations (5.1) and (5.2) in Table 1 describe the procedure followed in the model to analyze deposition by gravitation settling.

3.3.3 Deposition due to the combined effect of thermophoresis and diffusiophoresis: Thermophoresis, the motion of dispersed particles in a fluid medium due to a temperature gradient, occurs in a direction towards regions of lower temperature. Diffusiophoresis, the motion of dispersed particles due to a dissolved-component concentration gradient in a fluid medium, occurs in a direction towards a lower-concentration region. For a heat exchanger surface that is rejecting heat to the air stream, the temperature gradient established in the air would repel particles away from the heat exchanger surface; there would be no appreciable concentration gradient for any water vapor present in the air. Conversely, for a heat exchanger surface that is absorbing heat from the air stream, the

temperature gradient would attract particles to the heat exchanger surface. Water vapor present in the air may condense on the surface to establish a concentration gradient that also attracts particles to the surface. The thermophoretic and diffusiophoretic forces would act on suspended particulates in the same size range in the same direction and tend to be of the same order of magnitude [8]. Goldsmith and May [5] performed experiments to test whether thermophoresis and diffusiophoresis could be analyzed independently in this scenario, and reported that the forces acting on particles due to these two effects could be superimposed for aerosol deposition in helium or air. Assuming mutual independence between thermophoresis and diffusiophoresis may lead to an overprediction in the deposition rate because a certain particle could deposit under the combined action of both thermophoresis and diffusiophoresis.

Prediction of deposition due to thermophoresis (according to Talbot *et al.* [22]) and diffusiophoresis (according to Goldsmith and May [5]) is combined by superimposing the thermophoretic and diffusiophoretic forces. The net force acting on a particle in the direction of the surface is calculated, from which the net deposition velocity towards that surface is obtained. This velocity is used to calculate the deposition fraction of particles due to the net action of these two mechanisms. Equations (8.1) and (8.2) in Table 1 describe the calculation procedure employed in the model to find deposition due to net action of thermophoresis and diffusiophoresis.

3.3.4 Deposition due to turbulence: Particle transport due to turbulence is assumed to occur in two distinct ways – first due to entrainment occurring in turbulent flow, and second due to turbophoresis. In the first mechanism, dust particles are assumed to be entrained in secondary flows (in directions other than the bulk streamwise flow) resulting from formation of eddies, and in flows caused by random bursts of turbulent fluctuation velocity. Turbophoresis, the motion of dispersed particles in a fluid medium due to a difference in the local turbulence intensities, transports particles from regions of high to low turbulence. The analysis of deposition due to turbulence in the SN model used turbulence statistics from a direct numerical simulation of fully developed turbulent flow between parallel plates published by Moser *et al.* [28]. To better match operating conditions of field-installed heat exchangers and experiments, data should be extracted from simulation of representative duct geometries. The SN model considered deposition by turbulence as a two-dimensional phenomenon: deposition on fins from random velocity bursts in the horizontal spanwise direction and turbophoretic deposition on tubes in the streamwise direction for a heat exchanger installed in a duct with horizontal airflow. Turbulence in the vertical spanwise direction was assumed to not cause significant deposition. This assumption is logical for plain plate-finned-tube heat exchangers on account of the much smaller area available for deposition in the vertical spanwise direction as compared to that available in the horizontal spanwise direction. However, the fin corrugations in wavy finned tube heat exchangers could potentially provide surface area for particle deposition. The SN model assumed that turbulence from bulk flow in the duct does not persist into the airflow in the channels between the fins. Thus, deposition due to turbulence was only due to entrainment in random velocity bursts. For purposes of assessing the effect of the persistence of turbulence, turbulence from the upstream duct was alternatively assumed to persist through the entire depth of the heat exchanger; calculation of deposition with this turbophoresis was reported as an upper limit on deposition from turbulence-related mechanisms. While the narrow airflow channels could lead to some laminarization of the airflow, an absence of detailed turbulence data for airflow inside heat exchangers prevents the analysis of deposition due to turbulence induced by roughness elements and fin discontinuities within the heat exchanger itself (distinct from duct turbulence persisting inside the heat exchanger).

Figure 4 is a flow chart of the subroutine developed to predict particle deposition due to turbulence. Table 2 presents key equations used in the subroutine. The general approach for predicting deposition due to turbulence in the current study is similar to that of Siegel and Nazaroff [17] and uses a Monte Carlo simulation. However, because turbulence is a three-dimensional phenomenon, the modeling of deposition due to turbulence is extended to three dimensions for both mechanisms, as opposed to the two-dimensional approximation used in the SN model. Turbulence causes large deposition fractions for large particle sizes, and the extension of the analysis of deposition due to turbulence to three dimensions has a measureable influence on the total deposition fraction predicted. Turbulence statistics were reported by Gavrilakis [29] and Huser and Biringen [30] in all directions, and provided the numerical data necessary to perform this analysis. Regression curves were fitted to reported turbulence statistics such as primary and secondary velocity profiles, rms values of turbulent fluctuation velocities in all directions, and Reynolds stress profiles in all directions. Instantaneous turbulent fluctuation velocity was randomly sampled from a normal distribution about a mean of 0 and a standard deviation equal to the rms value of turbulent fluctuation velocity. Deposition due to turbulence in the additional vertical spanwise direction is modeled similarly to that in the horizontal spanwise and streamwise directions. The turbophoretic deposition is not used to define an upper limit on

deposition due to turbulence-related mechanisms as was done in the SN model; instead, its contribution is included in the prediction of actual deposition, instead of as an uncertainty estimate. The model approximates the hydrodynamic entrance length to be the length over which the duct turbulence persists inside the heat exchanger core. If the entrance length is greater than the depth of the first tube bank in the heat exchanger, then duct turbulence is assumed to persist inside the heat exchanger for the entire depth of the tube bank. The entrance length is approximated by the expression applicable for flow through rectangular ducts from McComas [31]. This persistence length is then used in the analysis of deposition due to turbophoresis. Equations (7.1), (7.2), (9), (10), and (11) in Tables 1 and 2 describe the computation procedure used to estimate deposition due to turbulence-related mechanisms.

3.3.5 Time-stepping to account for the effect of previously deposited dust on subsequent fouling: Based on fouling experiments with saw dust performed on a compact heat exchanger, Mason *et al.* [32] proposed distinct temporal regimes in the process of fouling. The increase in pressure drop across the heat exchanger as a function of time was divided into three phases. In the first *nucleation fouling* stage, the pressure drop increased gradually, and was followed by a second *transition fouling* stage, and finally with a *bulk fouling* stage during which the pressure drop increased very rapidly. Since saw dust was continuously injected into the air stream passing through the heat exchanger, this dependence on time reflects a dependence of the fouling rate on the extent to which the heat exchanger had been previously fouled. It was proposed that larger particles were deposited preferentially in the nucleation fouling stage. These deposits then acted as nucleation sites to trap smaller particles that would have otherwise passed through a clean heat exchanger.

House dust is a heterogeneous mixture of organic and inorganic particles and fibers of different sizes. Common sources of fibers in the air are paper, glass wool, wood, textiles [33], human hair and animal fur. Moore [34] studied the accumulation of fibrous dust on high-fin-density heat sinks. Due to the small fin pitches, the fibers formed bridges between adjacent fins. The resultant webbed structures were able to trap progressively finer particles, thus accelerating the process of fouling. In the case of compact finned heat exchangers increasingly common in HVAC&R applications, a similar phenomenon could lead to a progressive increase in the rates of fouling as a function of dust already present on the heat exchangers. Ahn and Lee [35] reported similar findings in prefilters; accumulated fibers formed dust-cake layers that acted as a secondary filtration medium and collected particles smaller than the filter pore sizes. Photographs of fouled condenser and evaporator heat exchangers which had been in service for periods between 3 to 14 years showed a significant presence of fiber and particulate agglomeration between the fins.

There are several other potential particulate-agglomeration-dependent deposition mechanisms. As air passages inside the heat exchanger become blocked by deposited dust, the distance that particles need to travel to impact upon the heat exchanger surface decreases. Surface deposits may also increase the turbulence inside the heat exchanger (Yang *et al.* [36]). These factors may contribute to progressively faster fouling of the heat exchanger over time. Bott and Bemrose [3] also asserted that the rate of deposit buildup is a function of the thickness of the fouling layer, which causes a change in the flow area and pattern through the heat exchanger, thus affecting the individual deposition phenomena. Hence the pressure drop across a fouled spiral wound finned tube heat exchanger increased at different rates depending on the dust concentration in the air stream (which influences the actual thickness of the deposited layer at the same deposition fraction). This deposit buildup mechanism is easily adapted into the deposition model, as done in the present work.

While there is no formal testing standard, experiments typically evaluate the fouling of heat exchangers by injecting dust into an air stream flowing through the heat exchanger at a set rate and duration. The injection of dust is then stopped and steady-state performance is measured in a fouled condition [3, 24, 36, 37, 38, 39, 40, 41]. Bott and Bemrose [3] claimed that the periodic nature of this testing approach does not affect the phenomenon of fouling. The deposition of dust on the heat exchanger is also evaluated by stopping air flow through the heat exchanger and measuring the mass of dust deposited. Continuous heat exchanger performance may also be measured to obtain transient behavior data as the surfaces are progressively fouled during testing [3, 42].

To mimic this experimental procedure for which data are available for comparison, dust deposition is modeled in discrete time periods corresponding to the periods of dust injection in the current approach. The modeling procedure approximates integral accumulation of dust by summing the deposition after each time step. When one time period ends, the total additional mass of dust deposited on the heat exchanger is calculated, and heat exchanger flow path

dimensions are modified to reflect the contraction due to fouling. This is achieved by artificially increasing the fin thickness and tube diameter of the heat exchanger based on the distribution of dust. The parameters dependent on the dimensions of the heat exchanger for flow past fins and tubes are recalculated based on the new dimensions. The model also checks for total blockage of flow passage due to fouling after a time step and returns a notification if this condition is reached.

3.3.6 Streamwise distribution of deposited dust: Large variations in the local streamwise distribution of deposited dust have been observed experimentally in the literature. Yang *et al.* [36] and Bell and Groll [37] observed that a majority of the fouled dust was deposited on the front face of the coil, and photographs showed that rear faces remained clean. Pak *et al.* [39] reported that dust accumulated more at the leading edges of fins, and that dust particles formed bridged shapes which reduced the front-facing open flow area. Ahn and Lee [35] reported that the fouling deposits were observed to have formed within 5 mm of the frontal air inlet to the heat exchanger surface, while the rear faces were fairly clean. Other experimental observations of concentrated fouling at the front face of the heat exchanger have been reported by Sun *et al.* [42] and Ali and Ismail [43].

The increase in pressure drop across the heat exchanger due to fouling is likely determined by deposition in the frontal region due to the greater local intensity of fouling. Similarly, if the front rows of the heat exchanger are heavily blocked due to dust deposition, the remaining rows of the heat exchanger could potentially remain clean even though the heat exchanger would not function properly. It is evident that modeling the distribution of the dust deposition inside a heat exchanger is important to predict the extent of fouling and its effect on performance, and the model results should reflect these experimental observations.

The SN model calculated the overall deposition fraction for the entire heat exchanger without considering its spatial distribution. In the current model, deposition due to each different mechanism is calculated in the streamwise direction in a discretized manner. Thus, the heat exchanger is divided into distinct sections; each section is composed of a tube row and a finned surface whose length is equal to the longitudinal tube pitch and which covers the entire height of the heat exchanger. This allows the mechanisms to naturally determine the distribution of deposition as a function of streamwise location along the heat exchanger. Such discretization of the calculation of deposition fraction due to each fouling mechanism in the streamwise length of air flow may possibly lead to a more accurate model for the distribution of deposited particulate matter.

To implement this streamwise distribution calculation in the model, once particulate matter is predicted to deposit in a particular section of the heat exchanger, the dust composition (both particle size and number of particles) in the air flowing through to the downstream section of the heat exchanger is updated. Thus, this discretization scheme not only yields information about the location of the deposition, but also affects the calculation of deposition fraction. Some mechanisms are governed by phenomena that behave nonuniformly over the cross section of the heat exchanger (*e.g.*, deposition due to turbulence is determined by local turbulence parameters). While these local phenomena are considered in calculating the total deposition fraction, the non-uniformity of the deposited layer is neither tracked nor considered in subsequent calculations. Assessment of the bulk density of the deposited dust layer (compared to the particle material density) is critical for accurate alteration of the heat exchanger dimensions as a result of its fouling in the time-stepping model. The particle density of the dust is obtained from the manufacturer data [44]. The bulk density of the deposited dust, however, could vary from the particle material density. The value currently used in the model is the bulk density of the test dust measured as received from the manufacturer (550 kg/m^3).

3.3.7 Effect of surface orientation on deposition mechanisms: The orientations of the heat exchanger surface geometries (with respect to gravity and the flow direction) uniquely influence each of the deposition mechanisms, and are also accounted for in the current model. Calculation of the inertial impaction on tubes and fins only considers the front halves of the tubes, whereas gravitational deposition only considers the top halves of tubes. It may be safely assumed that the lower halves of tubes need not be considered for the remaining mechanisms as a consequence of assumption *vii* (see Section 3.1). Thus, the region between the lowermost point of the tube and the trailing edge does not influence the calculation of any deposition mechanisms.

This approach is supported by prior experimental investigations. Abd-Elhady *et al.* [45] observed the build-up of fouling layers on heat exchanger tubes as a function of the direction of airflow with respect to gravity. They observed that fouling layers were thicker at the bottom rows of heat exchangers than at the top rows for all cases

(suggesting the influence of gravity). Fouling layers began at different locations on the tubes of heat exchangers and grew in different directions along the tubes depending on the direction of air flow and gravity. For all cases, fouling deposits were most likely to begin to grow at the stagnation point of airflow and the point on the top of the tube exactly in line with gravity. These layers then grew towards each other and merged.

Based on these experimental observations, the deposition fractions on the other radial locations were calculated according to the different mechanisms, taking into consideration the surface area on which deposition was likely in each case. Figure 5 shows the region of each fin and tube that was assumed to affect fouling by each individual deposition mechanism. The entire transverse surface areas of fins were assumed to be susceptible to fouling by all possible mechanisms. The front edges of fins were also assumed to be fouled as a result of inertial impaction of particles. While these surface-orientation-dependent regions of fouling are considered in calculation of the deposition fraction by each mechanism, the deposited dust is assumed to be uniform over the surface cross section for purposes of calculating the deposition layer thickness.

3.3.8 Streamwise changes in airflow dust composition: As a heat exchanger is fouled, the characteristics of the suspended particulates in the airflow change due to deposition. Not only does the total particulate concentration decrease due to fouling, but the particle sizes redistribute based on the size-dependent deposition mechanisms. This change affects the local deposition fraction at each individual tube row, and thereby alters the total overall deposition fraction for the heat exchanger. Consideration of the spatial variation of suspended particulate composition in the air stream is a logical extension of modeling the streamwise distribution of deposited dust, which also requires modeling the deposition in a discretized manner. The current model removes particulate matter from the air stream that is deposited on upstream heat exchanger sections and updates incident particulate dust composition for each discretized heat exchanger section.

4. RESULTS AND DISCUSSION

4.1 Experimental Results Used for Model Comparison

The experimental results of Pak *et al.* [39] and Yang *et al.* [36] are used for validating the model predictions; inputs required for the model regarding the heat exchanger geometry, such as the tube pitches in transverse and streamwise directions of airflow, fin pitches, and fin thickness, are available from these studies. In both sets of experiments, the heat exchangers to be tested were installed in a wind tunnel and connected to hot water loops for measuring the heat transfer performance. The inlet air temperature and inlet water temperature to the coils were both fixed and maintained constant for all tests. A commercially available dust injector (LMS Technologies, Inc.) was used to introduce dust into the wind tunnel at a constant rate. The injector aspirated the dust into a nozzle and sprayed it into the air stream by passing it through a perforated disc. The disk ensured that the dust was well-mixed and sprayed uniformly over the entire cross-section of the duct. The dust used was ASHRAE Standard Test Dust [46]. Each coil was loaded with dust for a pre-determined number of hours at 100 grams per hour. Additional details about each test are provided in Table 3. All heat exchangers with more than one tube row had a staggered arrangement of tubes.

In the experiments, filters placed downstream of the heat exchangers were used to catch dust particles that passed through the heat exchanger. The filter was weighed before and after each test to determine the amount of dust caught. The mass of dust injected into the air stream was known. Thus, the deposition fraction on the heat exchanger for the test could be experimentally determined as follows:

$$deposition\ fraction = \frac{mass\ of\ \ dust\ injected\ \ into\ the\ airstream - mass\ of\ \ dust\ caught\ \ in\ the\ downstream\ filter}{mass\ of\ \ dust\ \ injected\ into\ the\ airstream} \quad (12)$$

The experiments reported overall deposition fractions calculated over the entire duration of each test; the model updates the heat exchanger geometry on an hourly basis using on the deposition fraction calculated over each hour and then calculates a cumulative deposition fraction for the entire test period for comparison.

Figure 6 is adapted from data published by Flanders Corporation [47]. It shows the mass-based particle size distribution of ASHRAE Standard Test Dust. The particle size distribution that was originally published used broader particle diameter bins; for the current model input, these bins were uniformly subdivided to increase the resolution of particle sizes on the deposition. These more finely resolved particle size bins are indicated by the vertical lines subdividng the bars in Figure 6. The particle size bins with finer resolution are used because the

deposition fraction is a strong function of particle size; this approach yields a refined (and potentially more accurate) description of the particle sizes in the foulant buildup on the heat exchanger. ASHRAE test dust is a mixture of 72% by mass of ISO12103-1 A2 fine test dust, 23% powdered carbon, and 5% by mass of milled cotton linters. The particle density of the dust mixture was assumed to be a mass-fraction-weighted mean of the component particles. The calculated value of 2430 kg/m^3 is given here for reference and was used to perform the analysis reported in this work.

4.2 Model Predictions

To evaluate the contribution of each individual change in the model structure to a change in the predicted overall deposition fraction, a test case (2C, Table 3) was evaluated using the model at different intermediate stages of model development. The changes made were not reverted between different stages; therefore, each predicted deposition fraction reflects the cumulative impact of all prior changes. Figure 7 presents the deposition fraction predicted by different versions of the model; Table 4 lists short descriptions of the model enhancements referred to in Figure 7. The *SN model* described in Siegel and Nazaroff [17] was considered as the baseline. The changes listed in Table 4 are described in greater detail in Section 3.3.

The experimentally measured overall deposition fraction was approximately 58%. The baseline model (40.6%) underpredicted the experimental measurement. A superposition of thermophoresis and diffusiophoresis resulted in no significant change in the model prediction. A zone-based modeling of gravitational settling resulted in a minor decrease in the predicted overall deposition fraction (39.6%). This small change is probably a consequence of the stochastic nature of calculation of deposition from turbulence-related mechanisms. The new correlation used to calculate drag force acting on a dust particle resulted in no significant change in the model prediction. It should be noted that this change could potentially affect analysis of inertial impaction, gravitational settling, combined thermo- and diffusiophoresis, and deposition due to turbulence. However, the correlation is applicable only in the Newtonian regime and not in the Stokes regime. Thus, if particle motion did not fall within the Newtonian regime, a change in the correlation used to calculate drag force had no impact on the model prediction. For the current conditions investigated, the new drag force correlation was not anticipated to have a large impact; the new correlation was implemented because it includes the effects of particle shape and therefore can help in predicting the deposition of non-spherical particulates.

The largest change in the predicted deposition fraction occurred when the source of DNS velocity data for turbulent flow through a duct was updated to properly reflect flow through a 3D square duct (rather than the 2D channel geometry assumed in the SN model). The increase in predicted overall deposition fraction to 64.1% can be explained by one important factor. The DNS data used to assess deposition due to turbulence included information about secondary flows that exist in the duct. These secondary flow velocities, when added to the random velocity bursts, resulted in much higher calculated values for particle velocity towards the heat exchanger surface. Consequently, lower estimates were obtained for the time required for a particle to collide and deposit on the heat exchanger surface compared to the time required for a particle to pass through the heat exchanger core without collision. The extension of turbulent deposition to all directions resulted in a small further increase in the predicted overall deposition fraction to 66.5%. The relatively small change from the previous enhancement V can be explained by the fact that the calculation method accounted for scenarios that would erroneously double-count deposition of particles. That is, if a particle was predicted to deposit on fins due to a random velocity burst in the horizontal spanwise direction, deposition on a tube by turbophoresis in the streamwise direction was not counted again as an additional deposition event in the Monte Carlo simulation. The sample size of the Monte Carlo simulation was maintained at 10^7 cases to match the sample size of the simulation conducted by Siegel and Nazaroff [17].

Spatial discretization of the fouling model increased the predicted deposition fraction to 70.5%. This could be attributed to some additional deposition calculated on downstream tube banks, which is not explicitly accounted for in the baseline model. Temporal discretization of the fouling model resulted in a very slight increase in the predicted overall deposition fraction to 71%. This lower-than-expected contribution of accumulated deposition on fouling can be attributed to the fact that while the fouling agent contained 5% by mass of cotton fibers, the propensity of dust particles to be caught in these fibers was not accounted for in the model. In addition, the distribution of deposition was assumed to be completely uniform over the entire discretized section of the heat exchanger. However, this assumption is difficult to verify experimentally, and may not be applicable. It is possible that some regions in the heat exchanger were fouled to a greater degree than other regions in the experiment. Thus, a severely blocked airflow passage might aggressively agglomerate dust particles, which the model is not capable of predicting.

The progressive growth of deposition layers on the heat exchanger surface is shown in Figure 8 for a selected test case (2C, Table 3). The deposition layer for a tube row accounts for the deposition on the section of the heat exchanger corresponding to that row of tubes, *i.e.*, the surface area of the tube row and the finned area corresponding to the tube row. The model predicts that the front section of the heat exchanger will see a majority of the deposition, while the heat exchanger surface further downstream will remain relatively clean. This agrees with experimental observations reported in the literature [39, 36, 37, 35]. There is a small increase in the deposition fraction each hour as the heat exchanger is progressively fouled, from 70.4% during the first fouling period to 71.4% for the last period. This also qualitatively agrees with experimental observations, although the absolute increase in the deposition fraction with each hour is smaller than typically observed.
A comparison between experimental and calculated deposition fractions for the different test cases considered in Table 3 is presented in Figure 9. The calculated deposition fractions include predictions using the *SN model* and the model in its current form. The mean absolute error in the predicted deposition fraction decreases from 36.1% to 30.7% when prediction accuracy of the current model is compared to that of the SN model. In the first two cases, deposition due to turbulence was ignored by the model because the hydrodynamic entrance length for airflow between the fins was an order of magnitude smaller than the heat exchanger depth. Therefore, deposition due to turbulence was not calculated (in contrast to the SN model where turbulence was assumed to be independent of entrance length). Enhancements to the analysis of deposition from turbulence could improve prediction accuracy.

With inclusion of time-stepping in the calculated deposition fraction, in addition to other improvements made to the methods that estimate deposition due to each individual mechanism and their interactions, the overall deposition fraction predictions from the current model are closer (MAE of 31% compared to 36% for the SN model) to the experimental observations than the predictions from the SN model.

4.3 Sources of Discrepancy between Model and Experiment

4.3.1 Uncertainty in estimating experimental parameters: A primary potential source of error in the results is that some geometric parameters of the modeled heat exchangers have not been specified in the literature [39, 36]. Critical parameters including the fin thickness and dimensions of the louvers, lances, and wavy structures of the fins were estimated from published photographs or practical experience. The fin thickness for all cases was assumed to be 130 microns using measurements made on an outdoor unit for a commercial air conditioning system available in the authors' laboratory. To account for the louvers, the flow area blocked by the front edges of the louvers was added to the fin thickness; however, this addition does not accurately account for the increased deposition fraction observed experimentally on such surface enhancements. The effect of louvers is apparent in experimental results but accounting for the flows developed due to such surface enhancements is beyond the scope of this model.

4.3.2 Geometric complexity: Accounting for the various nonuniformly shaped structures that are used to increase turbulence inside the heat exchanger, such as louvers, in the model is complicated. For example, some of the louvers are cut out of the fin surface leaving open slits in the fin surface transverse to the airflow. These slits provide edges for deposition of dust; however, this deposition is not captured by the mechanisms included in the current model. Fouling of such slits has not been independently investigated in experiments. This is further complicated for experimental cases that have fins with both wavy structures as well as louvers, such as experimental cases 1C and 1D.

4.3.3 Particulate collisions and re-entrainment: The assumption that every collision of a dust particle with the surface results in deposition, as well as of an absence of re-entrainment of dust particles into the air stream, would induce some error in the model. To theoretically model these phenomena requires information about the intermolecular and electrostatic forces of attraction between dust particles and the metallic surfaces for all of the different constituents of the dust. Quantification of these forces would require extensive single-phenomenon data collection/validation for a variety of materials, and is outside the scope of the current work.

4.3.4 Bulk density of dust: The dust is a heterogeneous mixture of different components, and its bulk density is a function of the densities of its components weighted by their concentration, in addition to the porosity of the layer, which can easily change due to the deposition mixing process or moisture content. Thus, while the bulk density can be measured experimentally under controlled conditions, it cannot be deterministically calculated when modeling heat exchangers operated in the field, and serves as a potential source of uncertainty in modeling efforts. The bulk density of dust used to calculate the thickness of dust layers on the heat exchangers attempts to account for the agglomeration of dust particles that may occur due to humidity in the air and the actual physical process of impaction on the heat exchanger surface.

4.3.5 Distribution of prior fouling on surfaces: While the orientation of the surfaces is considered when calculating deposition by each mechanism, the distribution pattern of deposited particles is not known or accounted for. Little experimental data exist about the distribution patterns, which confounds modeling efforts. Such data could be obtained by collecting and weighing fouling on adjacent rows separately.

4.3.6 Turbulence inside the heat exchanger: Geometric enhancements on heat exchanger surfaces are meant to induce turbulence in the airflow. The internal geometry of heat exchangers where airflow patterns are repeatedly broken by tubes would also cause turbulence inside the heat exchanger. This turbulence could then cause deposition inside the heat exchanger. However, this information is not readily available in the published literature. It is difficult to predict particle deposition due to complex turbulence patterns in a fouling model that primarily uses deterministic calculations. A numerical-simulation-based model would be more suited for that purpose. In the present model, it was assumed that turbulence from flow inside a duct persists only a certain streamwise length into the heat exchanger. Thus, the contribution of this internally induced turbulence to deposition was neglected.

5. CONCLUSIONS

The model developed in this work is able to predict experimentally measured deposition fractions with improved accuracy relative to existing models, and could be used to evaluate fouling of HVAC&R heat exchangers of similar geometries as the test cases considered. The modified functionality of the model also enables approximation of the streamwise distribution of the deposited dust within the heat exchanger, and the effect of prior particle deposits on subsequent fouling (*i.e.*, temporal deposition characteristics). Due to the cumulative and combinatory nature of the approximations and assumptions made in the model, and on account of limited experimental data that only provide quantitative bulk deposition and qualitative descriptions of the dust distribution, more precise validation is difficult. In its current form, this model can be used to obtain reliable trends for the effects of different geometric and operating parameters on the fouling of heat exchangers. Rough estimates of the deposition fractions as a function of the heat exchanger geometry, thermophysical properties of air, and characteristics of the suspended particulate matter could then be used to avoid excessive fouling of fielded heat exchangers.

NOMENCLATURE

C_D = coefficient of drag, --

C_t = thermal exchange factor, --

D = momentum diffusion coefficient of air, m^2/s

D_{fin} = deposition due to inertial impaction on fins, --

D_{gra} = net deposition due to gravitational settling in wavy-finned-tube heat exchangers, --

$D_{gra,open}$ = deposition due to gravitational settling in open flow areas in the heat exchanger core, --

D_t = tube diameter, *m*

D_{tube} = deposition due to inertial impaction on tubes, --

D_{turb} = net deposition due to turbulence-related mechanisms, --

F_{diff} = diffusiophoretic force acting on a particle, *N*

d_p = particle diameter, *m*

H_w = height (double the amplitude) of one 'wave' in a wavy fin structure, *m*

C_s = thermal slip coefficient, --

$corf$ = correction factor for wavy fins, --

D_{bro} = deposition due to Brownian motion, --

$D_{ent,i}$ = deposition due to random bursts of turbulence along direction i, --

$D_{gra,corr}$ = deposition due to gravitational settling in corrugations, --

$D_{gra,plain-fins}$ = deposition due to gravitational settling in plain-finned-tube heat exchangers, --

D_t' = tube diameter corrected for deposition buildup, *m*

$D_{tur,i}$ = deposition due to turbophoresis along direction i, --

$D_{wv,air}$ = mass diffusion coefficient of water vapor in air, m^2/s

F_{ther} = thermophoretic force acting on a particle, *N*

$dist_i$ = distance to nearest heat exchanger surface in direction i, *m*

$J_{fl,i}$ = Lagrangian (or integral) diffusion scale of times along direction i, *s*

Kn = Knudsen number of particle flow, --

k_p = thermal conductivity of particle, *W/m-K*

M_{air} = molecular mass of air, *kg/kmol*

m_p = mass of particle, *kg*

N_t = number of transverse tube rows, --

P_t = transverse tube pitch, *m*

$p_{p,wv}$ = partial pressure of water vapor in air, *Pa*

St_{fin} = Stokes number for flow over fins, --

T_{air} = temperature of free stream of air, *K*

t'_{fin} = fin thickness adjusted for deposition buildup, *m*

U_{hx} = primary (streamwise) air velocity inside heat exchanger corrected for change in flow area, *m/s*

$u_{p,i}$ = instantaneous particle velocity along direction i (sum of mean and fluctuation velocities), *m/s*

u'_i = instantaneous turbulent fluctuation airflow velocity along direction i, *m/s*

$u'_{rms,i}$ = rms turbulent fluctuation airflow velocity along direction i, *m/s*

$u_{pho,i}$ = turbophoretic deposition velocity along direction i, *m/s*

$\overline{u'_i u'_j}$ = Reynolds stress in ij plane due to turbulent airflow, *N/m*^{2}

$w_{ther+diff}$ = net particle velocity under thermophoretic and diffusiophoretic forces towards fins, *m/s*

x_{wv} = mole fraction of water vapor in air, --

μ_{air} = dynamic viscosity of humid air, *kg/m-s*

$\nu_{t,air}$ = eddy diffusion coefficient (or eddy viscosity or turbulent viscosity), m^2-s

ρ_p = particle density, *kg/m*^{3}

$\tau_{imp,tur,i}$ = time needed for particle to collide with heat exchanger due to turbophoresis, *s*

∇n_{wv} = gradient of molar concentration of water vapor in air, *kmol/m*^{4}

∇T_{air} = gradient of temperature between air stream and heat exchanger surface, *K/m*

$\bigcup$ = logical OR operation

k_{air} = thermal conductivity of air, *W/m-K*

L_f = thickness of deposition layer, *m*

M_{wv} = molecular mass of water, *kg/kmol*

N_A = Avogadro constant, *1/kmol*

P_l = longitudinal tube pitch, *m*

P_w pitch (trough to trough distance) of one 'wave' in a wavy fin structure, *m*

S_{fin} = fin pitch, *m*

St_{tube} = Stokes number for flow over tubes, --

t_{fin} = fin thickness, *m*

U_{duct} = primary (streamwise) air velocity approaching heat exchanger, *m/s*

u_i = instantaneous airflow velocity along direction i (sum of mean and fluctuation velocities), *m/s*

$\overline{u}_i$ = mean airflow or particle velocity along direction i, *m/s*

$u'_{p,i}$ = instantaneous turbulent fluctuation particle velocity along direction i, *m/s*

$u'_{p,rms,i}$ = rms turbulent fluctuation particle velocity along direction i, *m/s*

u_s = settling velocity of particle under gravity, *m/s*

$v_{ther+diff}$ = net particle velocity under thermophoretic and diffusiophoretic forces towards tubes, *m/s*

x_{air} = mole fraction of air, --

ν_{air} = kinematic viscosity of humid air, m^2-s

ρ_{air} = density of humid air, *kg/m*^{3}

$\tau_{imp,ent,i}$ = time needed for particle to collide with heat exchanger due to entrainment in random velocity bursts, *s*

$\tau_{p,i}$ = relaxation time of particle for motion along direction i, *m/s*

∇p_{wv} = gradient of vapor pressure of water between air stream and heat exchanger surface, *Pa/m*

$\mathbb{P}$ = probability, --

REFERENCES

[1] Marner, W. J. (1990). Progress in gas-side fouling of heat-transfer surfaces. *Applied Mechanics Review, 43*(3), 35–66. doi: 10.1115/1.3101967

[2] *Particulate Matter (PM)*. (2013, March 18). Retrieved February 2, 2015 from United States Environment Protection Agency: http://www.epa.gov/airquality/particlepollution/

[3] Bott, T. R., & Bemrose, C. R. (1983). Particulate fouling on the gas-side of finned tube heat exchangers. *Journal of Heat Transfer, 105*(1), 178–183. doi: 10.1115/1.3245538

[4] Waldmann, L., & Schmitt, K. H. (1966). Thermophoresis and diffusiophoresis of aerosols. In C. N. Davies (Eds.), *Aerosol Science* (137–162). London: Academic Press. OCLC ID: 00627410

[5] Goldsmith, P., & May, F. G. (1966). Diffusiophoresis and thermophoresis in water vapor systems. In C. N. Davies (Eds.), *Aerosol Science* (163–194). London: Academic Press. OCLC ID: 00627410

[6] Derjaguin, B. V., Yalamov, Y. I., & Storozhilova, A. I. (1966). Diffusiophoresis of large aerosol particles. *Journal of Colloid and Interface Science, 22*(2), 117–125. doi: 10.1016/0021-9797(66)90072-5

[7] Annis, B. K., Malinauskas, A. P., & Mason, E. A. (1973). Theory of diffusiophoresis of spherical aerosol particles and of drag in a gas mixture. *Journal of Aerosol Science, 4*(4), 271–281. doi:10.1016/0021-8502(73)90087-6

[8] Pilat, M. J., & Prem, A. (1976). Calculated particle collection efficiencies of single droplets including inertial impaction, Brownian diffusion, diffusiophoresis and thermophoresis. *Atmospheric Environment, 10*(1), 13–19. doi: 10.1016/0004-6981(76)90253-5

[9] Davies, C. N. (1966). Deposition of aerosols from turbulent flow through pipes. *Proceedings of the Royal Society of London, Series A, Mathematical and Physical Sciences, 289*(1417), 235–246. doi: 10.1098/rspa.1966.0009

[10] Sehmel, G. A. (1970). Particle deposition from turbulent air flow. *Journal of Geophysical Research, 75*(9), 1766–1781. doi: 10.1029/JC075i009p01766

[11] Sehmel, G. A. (1971). Particle diffusivities and deposition velocities over a horizontal smooth surface. *Journal of Colloid and Interface Science, 37*(4), 891–906. doi: 10.1016/0021-9797(71)90370-5

[12] Sehmel, G. A. (1973). Particle eddy diffusivities and deposition velocities for isothermal flow and smooth surfaces. *Journal of Aerosol Science, 4*(2), 125–138. doi:10.1016/0021-8502(73)90064-5

[13] Cleaver, J. W., & Yates, B. (1976). The effect of re-entrainment on particle deposition. *Chemical Engineering Science, 31*(2), 147–151. doi: 10.1016/0009-2509(76)85049-X

[14] Kallio, G. A., & Reeks, M. W. (1989) A numerical simulation of particle deposition in turbulent boundary layers. *International Journal of Multiphase Flow, 15*(3), 433–46. doi: 10.1016/0301-9322(89)90012-8

[15] Epstein, N. (1988). Particulate fouling of heat transfer surfaces: Mechanisms and models. In L. F. Melo, T. R. Bott, & C. A. Bernardo (Eds.), *Fouling Science and Technology* (143–164). Dordrecht: Kluwer Academic Publishers. doi: 10.1007/978-94-009-2813-8

[16] Bott, T. R. (1988). Gas side fouling. In L. F. Melo, T. R. Bott, & C. A. Bernardo (Eds.), *Fouling Science and Technology* (191–203), Dordrecht: Kluwer Academic Publishers. doi: 10.1007/978-94-009-2813-8

[17] Siegel, J. A., & Nazaroff, W. W. (2003). Predicting particle deposition on HVAC heat exchangers. *Atmospheric Environment 37*(39), 5587–5596. doi: 10.1016/j.atmosenv.2003.09.033

[18] Hinds, W. (1982). *Aerosol Technology: Properties, Behavior, and Measurement of Airborne Particles*. New York: J. Wiley. ISBN: 9780471087267

[19] Wang, H. (1986). Theoretical adhesion efficiency for particles impacting a cylinder at high Reynolds number. *Journal of Aerosol Science, 17*(5), 827–837. doi: 10.1016/0021-8502(86)90036-4

[20] Pich, J. (1972). Theory of gravitational deposition of particles from laminar flows in channels. *Journal of Aerosol Science, 3*(5), 351–361. doi: 10.1016/0021-8502(72)90090-0

[21] DeMarcus W., and Thomas, J. W. (1952). *Theory of a diffusion battery*, (Oak Ridge National Laboratory Publication No. ORNL-1413) Oak Ridge, TN: U.S. Atomic Energy Commission. OSTI ID: 4393567

[22] Talbot, L., Cheng, R. K., Schefer, R. W., & Willis, D. R. (1980). Thermophoresis of particles in a heated boundary layer. *Journal of Fluid Mechanics, 101*(4), 737–758. doi: 10.1017/S0022112080001905

[23] Caporaloni, M., Tampieri, F., Trombetti, F., & Vittori, O. (1975). Transfer of particles in nonisotropic air turbulence. *Journal of the Atmospheric Sciences, 32*(3), 565–568. doi: 10.1175/1520-0469(1975)032<0565:TOPINA>2.0.CO;2

[24] Siegel, J. A. (2002). *Particulate fouling of HVAC heat exchangers* (doctoral dissertation). Mechanical Engineering Department, College of Engineering, Berkeley: University of California.

[25] Haider, A., & Levenspiel, O. (1989). Drag coefficient and terminal velocity of spherical and nonspherical particles. *Powder Technology, 58*(1), 63–70. doi: 0.1016/0032-5910(89)80008-7

[26] Seinfeld, J. H., & Pandis, S. N. (1998). *Atmospheric chemistry and physics: From air pollution to climate change*. New York: Wiley. ISBN: 978-0-471-72018-8

[27] Jennings, S. G. (1988). The mean free path in air. *Journal of Aerosol Science, 19*(2), 159–166. doi: 10.1016/0021-8502(88)90219-4

[28] Moser, R. D., Kim, J., & Mansour, N. N. (1999). Direct numerical simulation of turbulent channel flow up to Re = 590. *Physics of Fluids, 11*(4), 943–945. ISSN: 1070-6631

[29] Gavrilakis, S. (1992). Numerical simulation of low-Reynolds-number turbulent flow through a straight square duct. *Journal of Fluid Mechanics, 244*, 101–129. doi: 10.1017/S0022112092002982

[30] Huser, A., & Biringen, S. (1993). Direct numerical simulation of turbulent flow in a square duct. *Journal of Fluid Mechanics, 257*, 65–95. doi: 10.1017/S002211209300299X

[31] McComas, S. T. (1967). Hydrodynamic entrance lengths for ducts of arbitrary cross section. *Journal of Fluids Engineering, 89*(4), 847–850. doi: 10.1115/1.3609713

[32] Mason, D. J., Douch, N., & Heikal, M. R. (2002). Air side fouling of compact heat exchangers. In R. Stobart, P. R. N. Childs (Eds.), Proceedings of *The 2nd IMechE Automobile Division Southern Centre Conference on Total Vehicle Technology, Brighton, UK* (pp. 131–144). Brighton, UK: Professional Engineering Publishing. (Published as *Total Vehicle Technology: How Do We Get the Innovation Back into Vehicle Design)* ISBN 9781860583773

[33] Butte, W., & Heinzow, B. (2002). Pollutants in house dust as indicators of indoor contamination. *Reviews of Environmental Contamination and Toxicology, 175*, 1–46.

[34] Moore, D. A. (2009). Characterization of fiber accumulation fouling in fine pitched heat sinks. *25th Semiconductor Thermal Measurement and Management Symposium, San Jose, CA* (pp. 279–284). Piscataway, NJ: IEEE. doi: 10.1109/STHERM.2009.4810776

[35] Ahn, Y. C., & Lee, J. K. (2005). Characteristics of air-side particulate fouling materials in finned-tube heat exchangers of air conditioners. *Particulate Science and Technology, 23*(3), 297–307. doi: 10.1080/02726350590955930

[36] Yang, L., Braun, J. E., & Groll, E. A. (2007). The impact of fouling on the performance of filter–evaporator combinations. *International Journal of Refrigeration, 30*, 489–498. doi: 10.1016/j.ijrefrig.2006.08.006

[37] Bell, I. H., & Groll, E. A. (2011). Air-side particulate fouling of microchannel heat exchangers: Experimental comparison of air-side pressure drop and heat transfer with plate-fin heat exchanger. *Applied Thermal Engineering, 31*(5), 742–749. doi: 10.1016/j.applthermaleng.2010.10.019

[38] Haghighi-Khoshkhoo, R., & McCluskey, F. M. (2007). Air-side fouling of compact heat exchangers for discrete particle size ranges. *Heat Transfer Engineering, 28*(1), 58–64. doi: 10.1080/01457630600985675

[39] Pak, B. C., Groll, E. A., & Braun, J. E. (2005). Impact of fouling and cleaning on plate fin and spine fin heat exchanger performance. *ASHRAE Transactions, 111*(1), 496–504. ISSN: 0001-2505

[40] Bell, I. H., Groll, E. A., & König, H. (2011). Experimental analysis of the effects of particulate fouling on heat exchanger heat transfer and air-side pressure drop for a hybrid dry cooler. *Heat Transfer Engineering, 32*(3-4), 264–271. doi: 10.1080/01457632.2010.495618

[41] Lankinen, R., Suikonen, J., & Sarkomaa, P. (2003). The effect of air-side fouling on thermal-hydraulic characteristics of a compact heat exchanger. *International Journal of Energy Research, 27*(4), 349–361. doi: 10.1002/er.880

[42] Sun, Y., Zhang, Y., Barker, D., Ford, S., & Johnson, M. (2012). Experimental evaluation of air-side particulate fouling performance of heat exchangers. *ASHRAE Transactions 118*(1), 1116–1130. ISSN: 0001-2505

[43] Ali, A. H., & Ismail, I. M. (2008). Evaporator air-side fouling: Effect on performance of room air conditioners and impact on indoor air quality. *HVAC&R Research 14*(2), 209–219. doi: 10.1080/10789669.2008.10391004

[44] *ASHRAE 52.1 and 52.2 Test Dust Product MSDS Information*. (2012, November 2). Retrieved February 2, 2015 from Powder Technology Inc.: http://www.powdertechnologyinc.com/product-msds-information/

[45] Abd-Elhady, M. S., Rindt, C. C., & van Steenhoven, A. A. (2009). Optimization of flow direction to minimize particulate fouling of heat exchangers. *Heat Transfer Engineering, 30*(10–11), 895–902. doi: 10.1080/01457630902754142

[46] *Method of testing general ventilation air-cleaning devices for removal efficiency by particle size,* ANSI/ASHRAE Standard 52.2–2012. Atlanta, GA: American Society of Heating, Refrigerating, and Air-Conditioning Engineers, Inc. ISSN 1041-2336

[47] *Particle size distribution of ASHRAE test dust by mass*. (2003). Retrieved February 2, 2015 from Flanders Corporation website: http://www.flanderscorp.com/files/Technical_Data/ASHRAE+DUST+SIZE+DISTRIBUTION.pdf

[48] Muzychka, Y. S. & Yovanovich, M. M. (2002). Laminar flow friction and heat transfer in non-circular ducts and channels: Part I – Hydrodynamic problem. In G. P. Celata, B. Thonon, A. Bontemps, S. Kandlikar (Eds.), Proceedings of *International Symposium on Compact Heat Exchangers, Grenoble, France* (pp.

123–130). Pisa, Italy: Edizioni ETS. (Published as *Compact Heat Exchangers: A Festschrift on the 60th Birthday of Ramesh K. Shah*) ISBN: 9788846706195

[49] Sonnad, J. R. & Goudar, C. T. (2007). Explicit reformulation of the Colebrook-White equation for turbulent flow friction factor calculation. *Industrial and Engineering Chemistry Research, 46*(8), 2593–2600. doi: 10.1021/ie0640241

ACKNOWLEDGEMENT

This study was funded by members of the Cooling Technologies Research Center, an NSF Industry/University Cooperative Research Center at Purdue University.

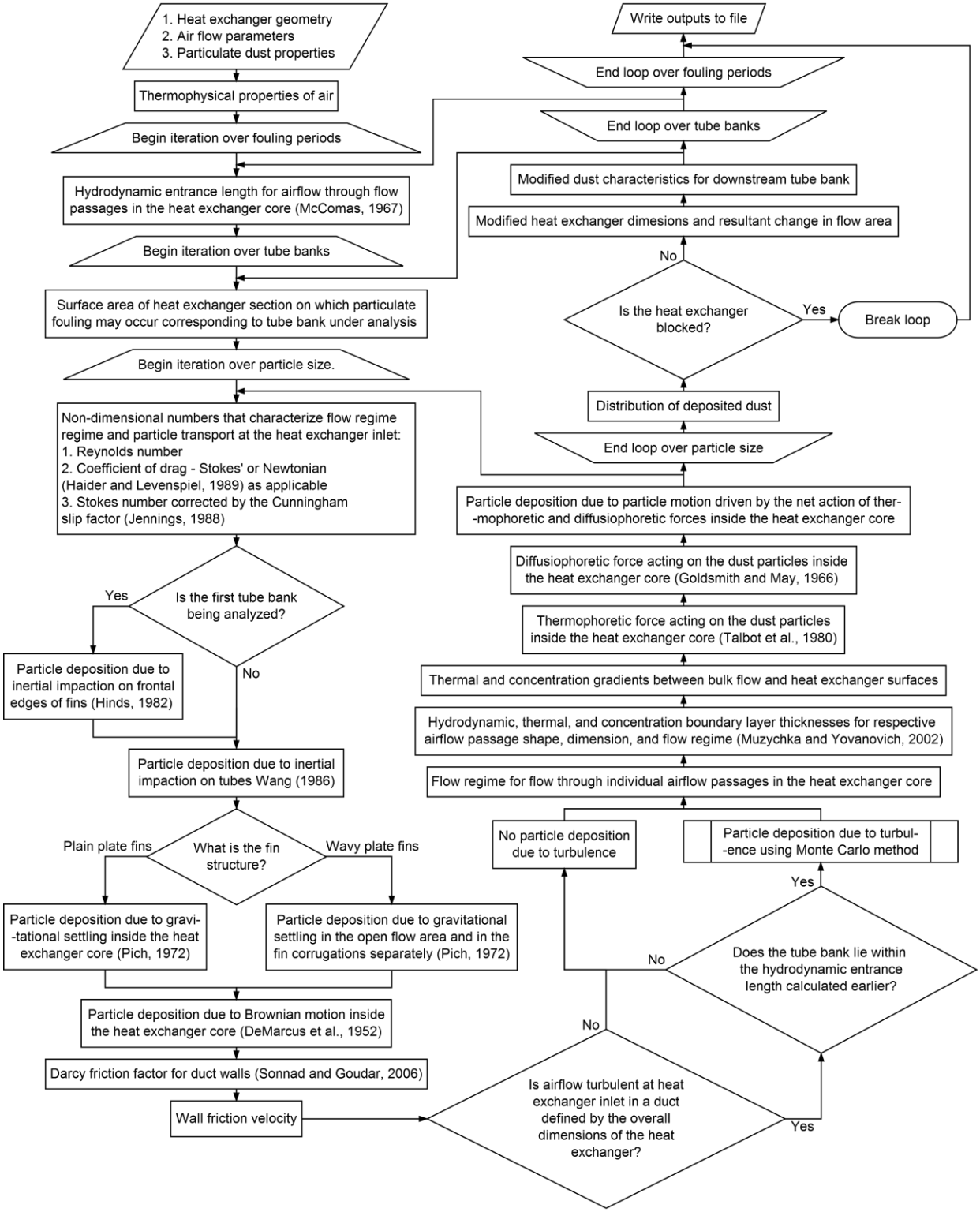

Figure 1. Flow chart of analytical model developed to predict fouling of an HVAC&R heat exchangers.

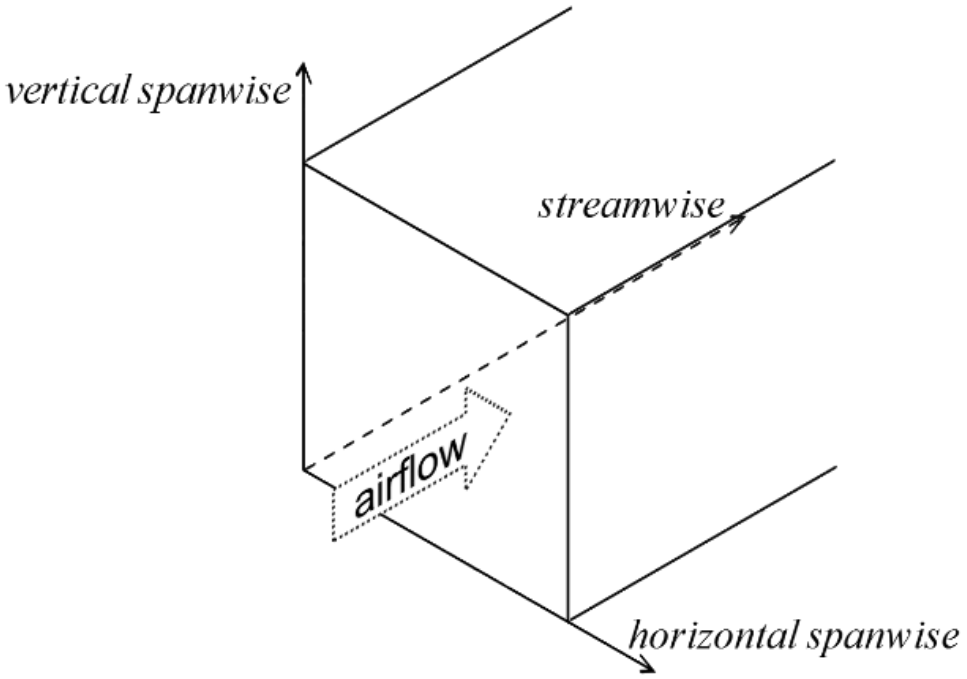

Figure 2. Naming convention used to denote directions with respect to the duct.

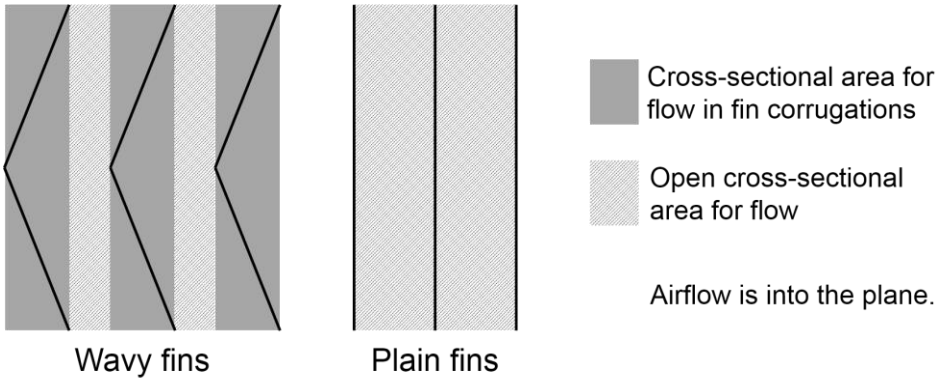

Figure 3. Schematic division of airflow passages into distinct gravitational settling zones.

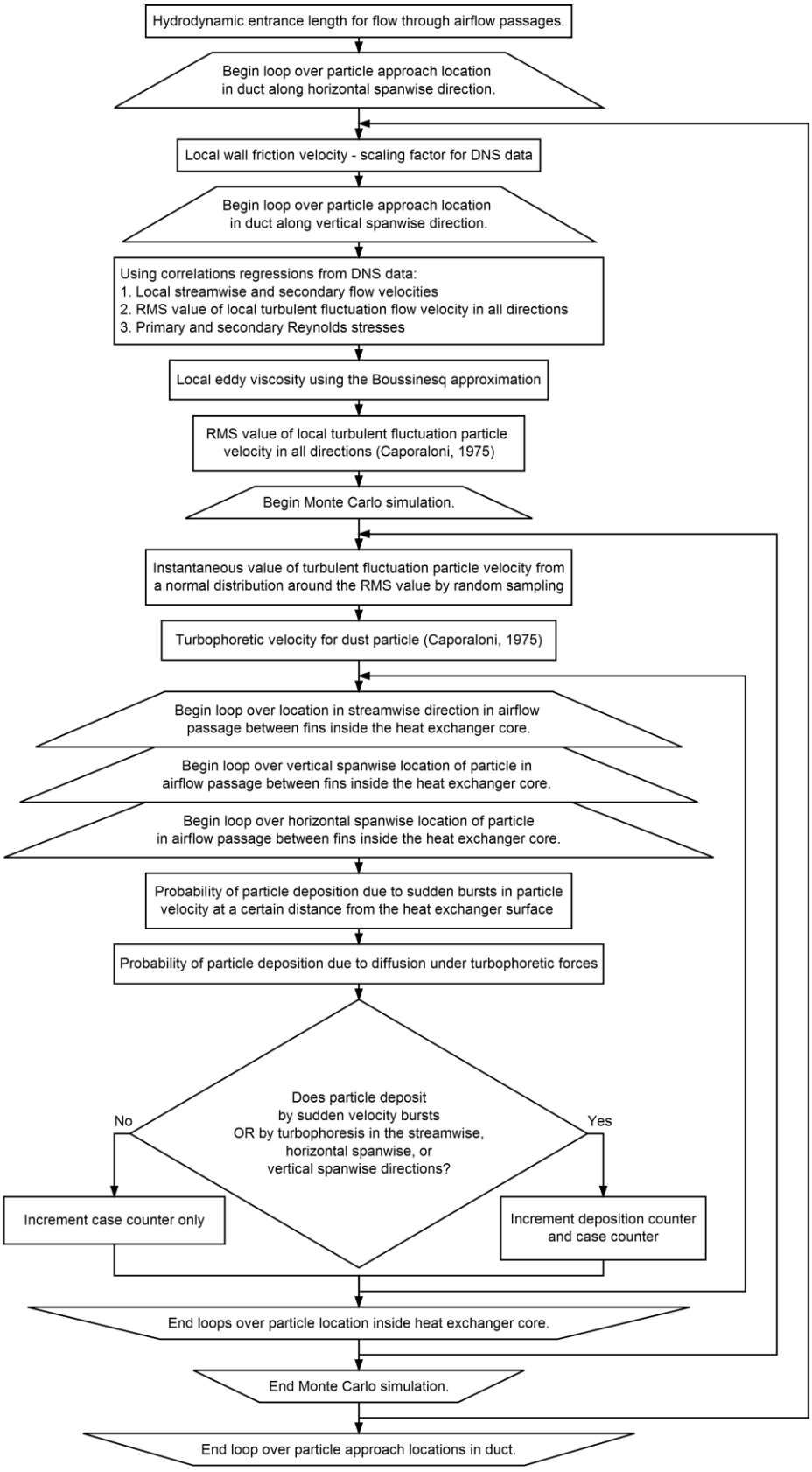

Figure 4. Flow chart of subroutine used to evaluate fouling due to turbulence driven deposition mechanisms.

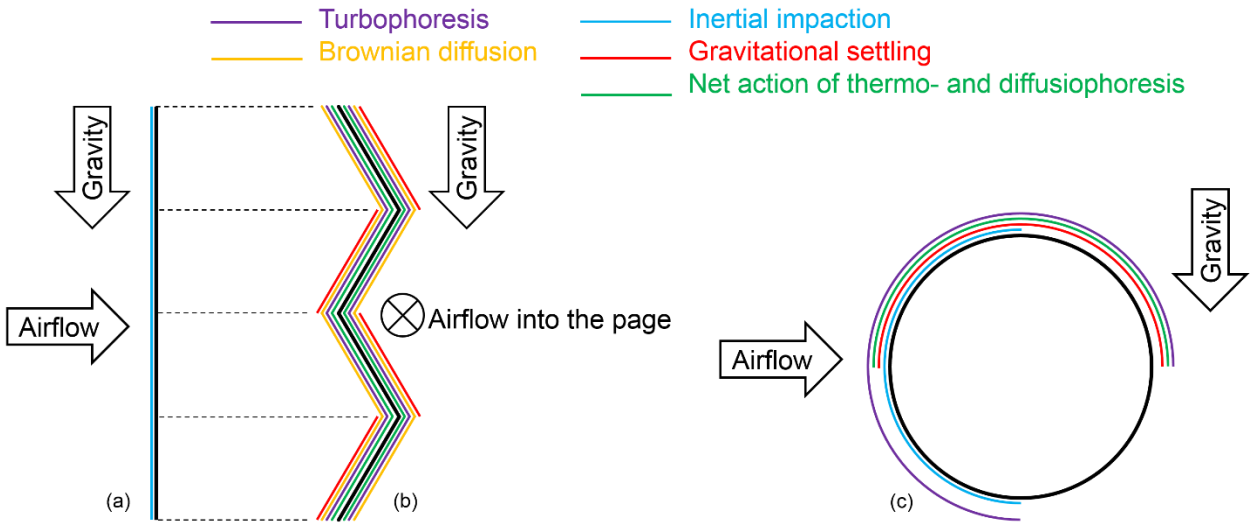

Figure 5. Assumed distribution of deposited dust, based on each deposition mechanism, on a wavy fin (as seen from its side (a) and from the front (b)) and on (c) a heat exchanger tube as seen from the side.

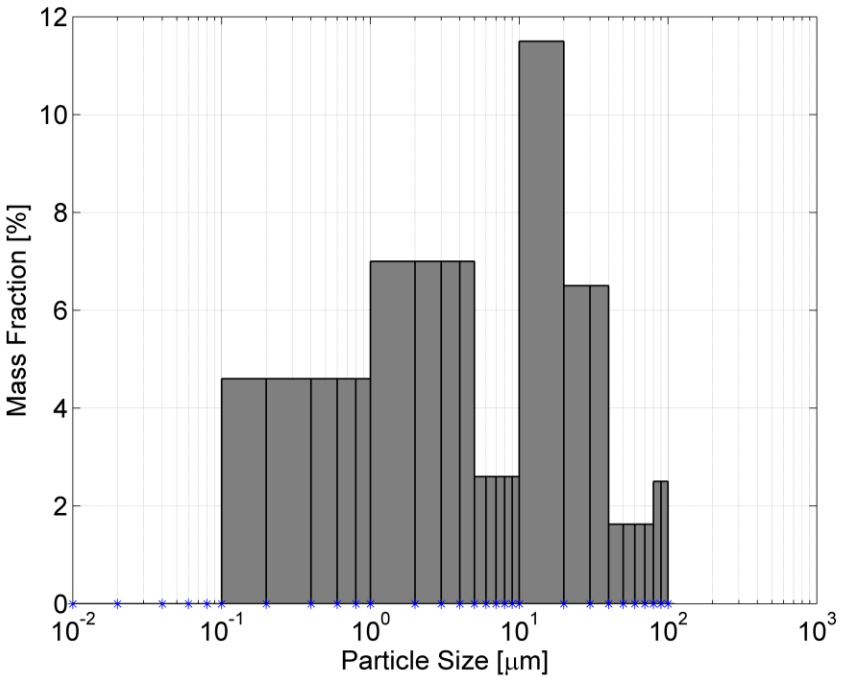

Figure 6. Mass-based particle size distribution of ASHRAE Standard Test Dust used in the fouling model.

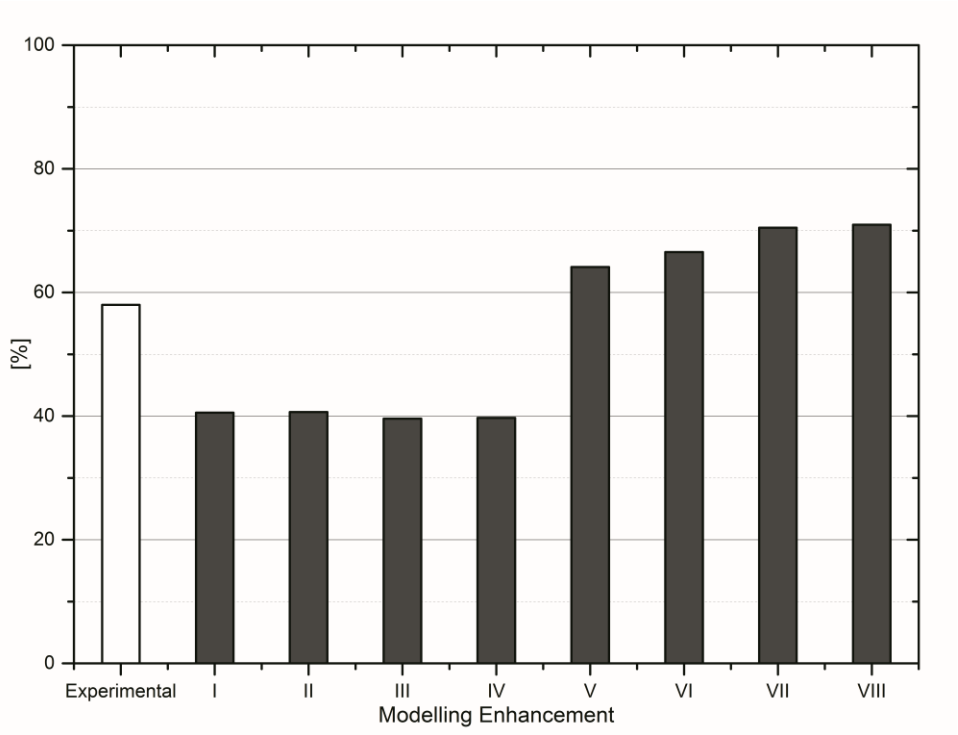

Figure 7. Change in predicted deposition fraction due to changes made in the model as listed in Table 4.

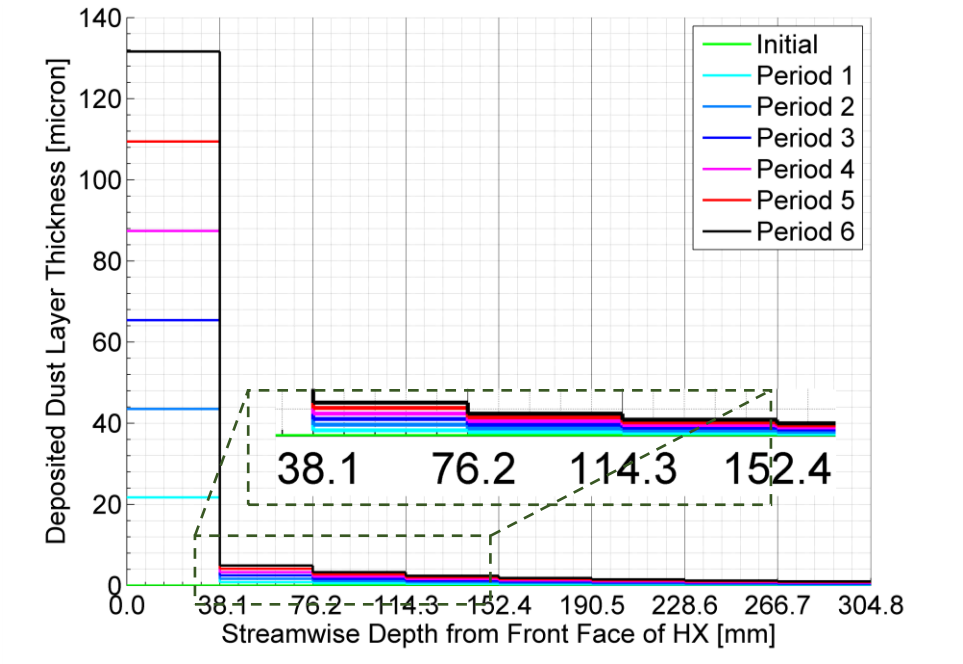

Figure 8. Thickness of deposition layer formed on the heat exchanger surface as a function of the streamwise depth from front face and time (Test 2C).

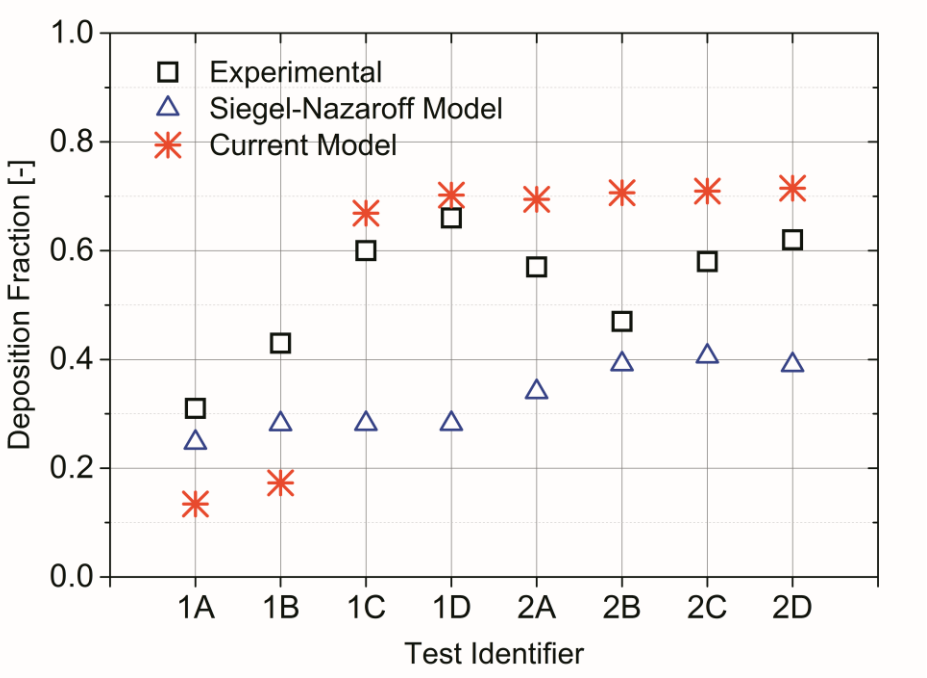

Figure 9. Comparison of experimental and calculated deposition fractions from both models.

Table 1. Important equations used to calculate deposition due to each mechanism in the current model.

Deposition Mechanism	Equation for Deposition Fraction		Definitions	
Inertial impaction on fins [18]	$D_{fin} = \min\left(1\ ,\ St_{fin} \cdot \frac{\pi}{2}\right) \times \frac{t'_{fin} \cdot corf}{S_{fin}}$	(3.1)	$St_{fin} = \tau_{p,x} \cdot \frac{U_{duct}}{t'_{fin}}$	(3.2)
Inertial impaction on tubes [19]	$D_{tube} = \min\left\{1\ ,\ \frac{2}{\pi} \times \tan^{-1}\left[0.8\left(St_{tube} - \frac{1}{8}\right)^{0.8}\right]\right\} \times \frac{D'_t}{P_t}$	(4.1)	$St_{tube} = \tau_{p,x} \cdot \frac{U_{duct}}{D'_t}$	(4.2)
Gravitational settling [20]	$D_{gra,plain-fins} = \frac{u_s \cdot P_l}{U_{hx} \cdot N_t \cdot P_t}$ $D_{gra,open} = \frac{u_s \cdot P_l \times \left(S_{fin} - H_w\right)}{U_{hx} \cdot N_t \cdot P_t \times \left(S_{fin} - t'_{fin} \cdot corf\right)}$ $D_{gra,corr} = \frac{u_s \cdot P_l \times \left(H_w - t'_{fin} \cdot corf\right)}{\left(\frac{P_w - 2 \cdot L_f / corf'}{2}\right) \times U_{hx} \times \left(S_{fin} - t'_{fin} \cdot corf\right)}$ $D_{gra} = D_{gra,open} + D_{gra,corr}$	(5.1)	$corf' = \sqrt{1 - \frac{1}{corf^2}}$	(5.2)
Brownian diffusion [21]	$D_{bro} = 0.91489 \times \exp\left(-2.827785 \cdot \phi\right) + 0.059245 \times \exp\left(-33.5 \cdot \phi\right)$ $+0.025865 \times \exp\left(-227.672 \cdot \phi\right)$	(6.1)	$\phi = \frac{8 \cdot D \cdot P_l}{3 \cdot U_{hx} \cdot \left(S_{fin} - t'_{fin}\right)^2}$	(6.2)
Turbulence-related mechanisms (adapted from [17])	$D_{ent,i} = \mathbb{P}\left(\frac{\tau_{imp,ent,i}}{\tau_{p,i}} < 1\right)$ $D_{tur,i} = \mathbb{P}\left(\frac{\tau_{imp,tur,i}}{\tau_{p,i}} < 1\right)$ $D_{turb} = \mathbb{P}\left[\left(D_{ent,x} \cup D_{pho,x}\right) \cup \left(D_{ent,y} \cup D_{pho,y}\right) \cup \left(D_{ent,z} \cup D_{pho,z}\right)\right]$	(7.1)	$\tau_{p,i} = \frac{\left\lvert u_{p,i} - u_i \right\rvert \cdot m_p}{F_{drag,i}}$ $\tau_{imp,ent,i} = \frac{dist_i}{u_{p,i}} = \frac{dist_i}{\bar{u}_i + u'_p}$ $\tau_{imp,pho,i} = \frac{dist_i}{\bar{u}_i + u_{pho,i}}$	(7.2)

Thermo- and diffusiophoresis [5, 22]

$$F_{diff} = -\frac{\sqrt{M_{wv}} \times D_{wv,air}}{x_{wv} \times \sqrt{M_{wv}} + x_{air} \times \sqrt{M_{air}}} \times \frac{1}{p_{p,wv}} \times \nabla p_{wv} \cdot 3\pi \cdot \mu_{air} \cdot d_p \quad \text{for } Kn < 0.6$$

$$F_{diff} = -\frac{D_{wv,air} \times \left(M_{wv} - M_{air}\right)}{\rho_{air} \cdot N_A} \times \nabla n_{wv} \cdot 3\pi \cdot \mu_{air} \cdot d_p \quad \text{for } Kn \geq 0.6$$

$$F_{ther} = -\frac{6\pi \cdot \mu_{air} \cdot \nu_{air} \cdot d_p \cdot C_s \times \left(k_{air} \big/ k_p + C_t \cdot \mathrm{Kn}\right) \nabla T_{air}}{\left(1 + 3 \cdot C_m \cdot \mathrm{Kn}\right) \times \left(1 + 2 \cdot k_{air} \big/ k_p + C_t \cdot \mathrm{Kn}\right) \times T_{air}}$$

$$D_{ther+diff,\,fin} = \frac{2 \cdot P_l \cdot w_{ther+diff}}{U_{hx} \times \left(S_{fin} - t'_{fin} \cdot corf\right)}$$

$$D_{ther+diff,\,tube} = \frac{D'_t \cdot v_{ther+diff}}{U_{hx} \times \left(P_t - D'_t\right)}$$

(8.1)

$$F_{diff} + F_{ther} = F_{drag}$$

$$v_{ther+diff} = w_{ther+diff}$$

(8.2)

$$F_{drag} = \frac{C_D}{C_C} \cdot \frac{\pi}{8} \cdot \rho_{air} \cdot {d_p}^2 \cdot {w_{ther+diff}}^2$$

Table 2. Additional equations used in the model to analyze deposition due to turbulence.

Variable Evaluated	**Equation**	
Turbophoretic velocity [23]	$u_{pho,i} = -\tau_{p,i} \frac{\partial u'^2_{rms,i}}{\partial x}$	(9)
Particle turbulent fluctuation velocity [23]	$u'^2_{p,rms,i} = K u'^2_{rms,i}$ where, $K = \frac{aJ_{fl,i} + b^2}{aJ_{fl,i} + 1}$ such that $a = \frac{36\mu_{air}}{\left(2\rho_p + \rho_{air}\right) d_p^2}$ and $b = \frac{3\rho_{air}}{2\rho_p + \rho_{air}}$	(10)
Lagrangian (or diffusion) integral scale of times [23]; Eddy diffusion coefficient (or eddy viscosity or turbulent viscosity) (Boussinesq approximation)	$J_{fl,i} \approx \frac{\nu_{t,air}}{u'^2_{rms,i}}$ where $-\overline{u'_i u'_j} = \nu_{t,air}\left(\frac{\partial \overline{u}_i}{\partial x_j} + \frac{\partial \overline{u}_j}{\partial x_i}\right)$	(11)

Table 3. Summary of operating parameters of experiments used for comparison against model predictions.

Study	Test Identifier	Tube Parameters (mm)	Number of Rows	Fin Type	Fin Density (fins per inch, FPI)	Dust Type	Duration of Test (hr)
Pak *et al.* [39]	1A	D_t = 9.52 P_t = 30.5 P_l = 30.5	1	Plain plate	22	ASHRAE Standard Test Dust	3
	1B	D_t = 9.52 P_t = 30.5 P_l = 30.5	1	Louvered wavy plate	22		3
	1C	D_t = 9.52 P_t = 30.5 P_l = 30.5	2	Louvered wavy plate	22		3
	1D	D_t = 9.52 P_t = 30.5 P_l = 30.5	2	Louvered wavy plate	22		3
Yang *et al.* [36]	2A	D_t = 9.52 P_t = 22 P_l = 25.4	2	Lanced plate	14		6
	2B	D_t = 12.7 P_t = 33 P_l = 38.1	4	Lanced plate	12		6
	2C	D_t = 12.7 P_t = 33 P_l = 38.1	8	Wavy plate	8		6
	2D	D_t = 12.7 P_t = 33 P_l = 38.1	8	Lanced plate	8		6

Table 4. Description of improvements to the model in stages to assess the impact of each subsequent change relative to the SN model.

Modeling Enhancement	Description
I	Baseline: SN model replicated
II	Thermophoretic and diffusiophoretic forces superimposed
III	Zone-based analysis of gravitational settling implemented
IV	Correlation used to calculate drag coefficient enhanced
V	DNS data updated for turbulent flow through the experimental square-duct geometry
VI	Deposition due to turbulence calculated along all directions
VII	Heat exchanger discretized spatially
VIII	Process of fouling discretized temporally